

Large Growth Rayleigh-Taylor Experiments Using Shaped Laser Pulses

B. A. Remington, S. W. Haan, S. G. Glendinning, J. D. Kilkenny, D. H. Munro, and R. J. Wallace

Lawrence Livermore National Laboratory, Livermore, California 94550

(Received 18 January 1991)

Large growth Rayleigh-Taylor (RT) experiments have been conducted by pulse-shaped radiative acceleration of planar fluorosilicone foils with 50- μm -wavelength initial surface perturbations. Foils with large-amplitude initial perturbation quickly enter the nonlinear RT regime, and show little growth. Foils with very-small-amplitude initial perturbations grow exponentially for longer, and show much larger growth factors. From comparisons with two-dimensional computer simulations, we deduce that the observed growth is about 60% of that expected for classical RT growth.

PACS numbers: 52.35.Py, 52.65.+z, 52.70.-m

Hydrodynamic instabilities [1] play a pivotal role in current approaches to inertial confinement fusion [2] (ICF). In the direct drive approach [2-4], multiple lasers simultaneously illuminate the outer surface of a spherical capsule vaporizing the ablation layer, causing the inner pusher layer to accelerate inward. This compresses and heats the nuclear fuel contained inside initiating fusion and the release of energy. In indirect drive, lasers [5,6] or ion beams [7] first convert to x rays inside a high-Z enclosure (hohlraum), which then drive the implosion. Regardless of approach, a low-density plasma blowoff accelerates a higher-density pusher at the ablation front; hence, capsule surface imperfections will grow due to the Rayleigh-Taylor (RT) instability [1-4,8]. Sufficient perturbation growth can lead to shell breakup or seed perturbations on the inner surface of the shell which in turn grow during the deceleration phase, degrading capsule performance. High-gain capsule designs [2-5,7,8] call for shaped drive pulses and large aspect ratios (radius/wall thickness) to maximize the implosion hydrodynamic efficiency. The steep density gradient, thin capsule wall, and extended acceleration phase of these high-gain designs, however, create a particularly suitable environment for large RT growth [3]. Experiments of perturbation growth in this environment are crucial to the fate of ICF.

Experiments to date have measured RT growth on planar foils accelerated by direct laser illumination [9], by illumination with smoothed laser pulses [10], by indirect drive using 1-ns-square laser pulses [11], and by direct drive implosions [12]. Though the amount of growth typically observed was limited and the drive pulse shapes rather arbitrary, the measured RT growth rates were somewhat reduced from classical. The extent to which surface imperfections grow in an extended, shaped acceleration, however, is still a very open question. We report here the first experimental measurements of RT growth using a pulse-shaped drive similar to a scaled version of those being considered for high-gain implosions. In this series the drive, foil thickness, and perturbation wavelength were held fixed, and only the perturbation amplitude was varied, with the smallest value approaching the scale of typical surface imperfections.

The experimental setup is illustrated in Fig. 1. A sinusoidal surface perturbation of wavelength 50 μm is

imposed on one side of a 750- μm -diam fluorosilicone ($\text{SiOC}_4\text{H}_7\text{F}_3$) planar foil. Fluorosilicone (FS) was chosen because this admixture of opacities allows an extended acceleration period without early foil burn through or decompression due to preheat. The uncertainties in foil thickness, perturbation wavelength, and amplitude are estimated to be $\pm 2\%$, $\pm 2\%$, and $\pm 10\%$, respectively. The foil is mounted across a hole in the wall of a gold cylindrical hohlraum with the perturbations facing inwards, and accelerated as shown schematically in the figure for face-on geometry. The perturbation growth is measured by x-ray backlighting onto a streaked Wölter x-ray microscope (the "22 \times ") [13]. The spatial and temporal resolution of the 22 \times and streak camera are approximately 10 μm and 150 ps in these experiments. The x-ray drive was generated by focusing eight 0.35- μm , 2.2-kJ, 3.2-ns Nova [5] beams into the hohlraum. The ablation pressures thus generated in the foil are measured in separate shock-breakout experiments [5] and are a factor of several larger than for typical direct drive experi-

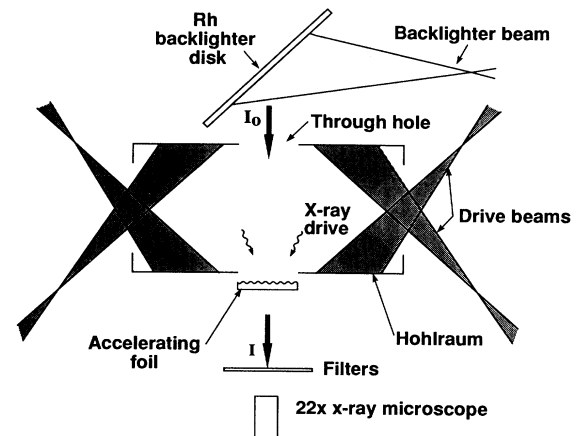


FIG. 1. Schematic of the experimental setup (not to scale). The foil is mounted on the wall of a cylindrical gold hohlraum with surface perturbation facing inwards, and eight drive laser beams entering the ends of the hohlraum generate an x-ray drive. As the foil accelerates by x-ray ablation towards the 22 \times magnification x-ray microscope, another laser beam striking a backlighter disk generates a back illumination of x rays which traverse the hohlraum and the accelerating foil. Modulations in foil areal density translate to modulations in exposure at the x-ray camera.

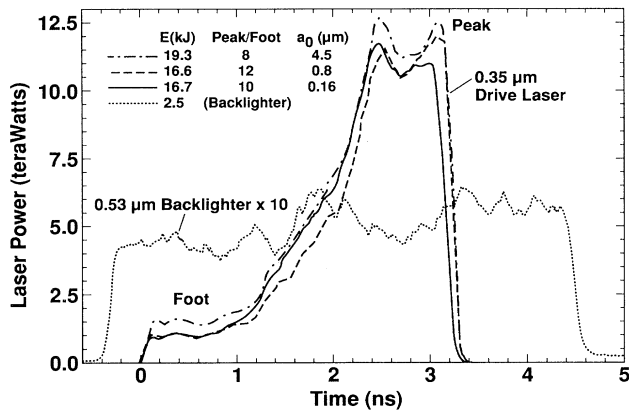


FIG. 2. Total power, summed over the eight 0.35- μm drive lasers, for each shot in the amplitude (a_0) scaling series. A backlighter pulse typical for the series is shown by the dotted curve.

ments [9,10]. The laser pulse shape, shown in Fig. 2, has a contrast of peak/foot ≈ 10 . This shape is designed to minimize the shock heating and subsequent decompression of the foil [5], as in high-gain implosion designs [2-4,7,8]. The foil was backlit with a 750- μm -diam spot of x rays created by irradiating a dysprosium or rhodium disk with a ninth Nova beam of wavelength, shape, and energy of 0.53 μm , 5 ns square, and 2.5 kJ, respectively. After including the 22 \times response, the dominant feature in the backlighter spectrum is a band of x rays at 1.5-1.9 keV for Dy and 2.7-3.2 keV for Rh. The growing modulations in the foil areal density cause modulations in the x-ray optical depth and hence in the exposure at the image plane of the detector which are recorded as a function of time by the streaked 22 \times . The image begins promptly when the backlighter beam turns on, and the relative timing between the backlighter beam and the drive beams is measured on optical and on UV streak cameras on each shot, thus establishing $t=0$.

Figure 3 shows $\ln(\text{exposure})$ profiles for an accelerated thin FS foil with a large-amplitude (1.9 μm) initial perturbation. The peak-to-valley modulation in these curves will be referred to as "contrast." This representation of the data is chosen because exposure $\propto e^{-\kappa\rho_a}$, where κ represents average opacity and $\rho_a = \int \rho dz$ is the foil areal density. Hence, $\ln(\text{exposure}) \propto -\kappa\rho_a$ and growth in contrast is equivalent to growth in foil $\int \rho dz$. At early times the contrast is small and sinusoidal in shape, indicating that the RT instability is in the linear regime. Late in time, the contrast is greater and distinctly nonsinusoidal, exhibiting the "bubble-and-spike" shape characteristic of the nonlinear RT regime [8]. The flattening of the modulations in the top curve results from burn through, when the bubbles have broken out the back side of the foil.

The foil trajectory was measured by observing a thick FS foil edge-on as it accelerates across and progressively blocks the backlighter spot. A trajectory can be constructed [14] by following the point where the optical

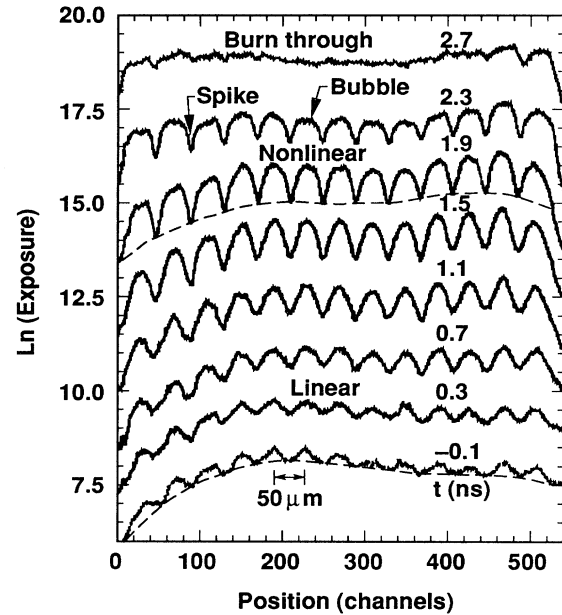


FIG. 3. Measured $\ln(\text{exposure})$ curves vs time for an accelerated thin fluorosilicone foil with an initial 50- μm -wavelength, 1.9- μm -amplitude sinusoidal surface perturbation, and a Dy backlighter. Each curve represents the average over a 400-ps time interval, and is offset vertically from bottom to top in order of increasing time. Three phases of the foil evolution (linear, nonlinear, burn through) are indicated, as are typical examples of "bubble" and "spike." The dashed curves represent an estimate of the average long-range structure due to backlighter nonuniformity.

depth (OD) of the back edge increases above the baseline by some $\delta(\text{OD})$. Averaging over the ensemble generated by varying $\delta(\text{OD})$ over the range 0.25-1.50, we show the average foil trajectory in Fig. 4(a). The back edge of the foil does not start to accelerate until the shock breaks out at about 2.5 ns. The drive lasers turn off at 3.2 ns, after which the foil moves at approximately constant velocity. Also shown is the corresponding trajectory from one-dimensional simulations using the computer code LASNEX [15]. (The essential features of LASNEX have been compared extensively with theory [16] and with results of experiments on Nova [5].) The simulations use a measured x-ray drive spectrum. We also show from the simulations the evolution of the acceleration of the zone of peak density.

In our amplitude scaling series, we accelerated in face-on geometry thick FS foils with initial amplitude a_0 of 4.5, 0.8, and 0.16 μm . The periodic modulations in $\ln(\text{exposure})$ were Fourier analyzed, and the coefficient of the fundamental mode for each experiment is shown in Fig. 4(b). For the foils with large a_0 (4.5 μm) and with intermediate a_0 (0.8 μm), contrast was observable throughout the experiment, including at $t=0$ when the drive beams just turn on. For the small a_0 (0.16 μm) foil, initial contrast was not resolved but can be calculated very reliably [14]. The perturbation for the large a_0

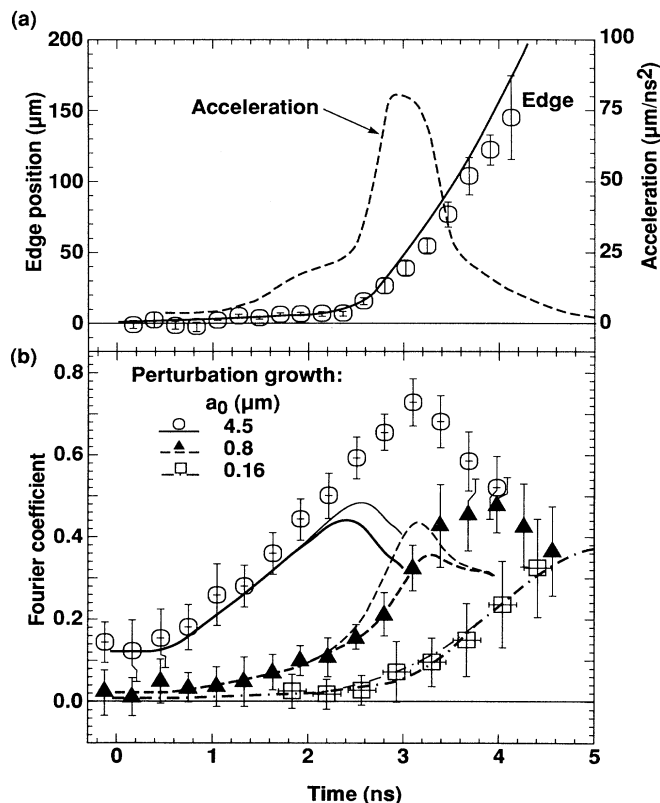


FIG. 4. (a) The average trajectory of the foil back edge, measured in edge-on geometry using a Rh backlighter. The solid curve represents the corresponding one-dimensional trajectory simulation with the computer code LASNEX. The dashed curve gives the acceleration of the zone of peak density from the simulation (scale given on right). (b) The fundamental Fourier-transform coefficient of $\ln(\text{exposure})$, measured in face-on geometry with a Rh backlighter, for accelerated foils with large (circles, solid curves), intermediate (triangles, dashed curves), and small (squares, dash-dotted curves) initial amplitude perturbations. The error bars represent the standard deviation of the Fourier transforms of the individual periods at each time bin. The smooth curves are the results of two-dimensional LASNEX simulations. The thick curves assume constant backlighting from the backlighter disk only; the thin curves include an additional transitory contribution from hohlraum emission.

foil appears to be growing nearly linearly between 0.5 and 3.0 ns, then starts to decrease. The second and third harmonics appear [14] (not shown here) at about 1.5 and 3.3 ns and grow to peak values of 38% and 18% of the peak value of the fundamental, indicating that the perturbation has evolved into the bubble-and-spike nonlinear RT phase [8]. Indeed, the “roll over” in the fundamental mode is probably because the spikes are becoming too narrow to resolve with the $22\times$. For the intermediate a_0 foil, the growth appears to be nearly exponential until about 3.3 ns, then rolls over and starts to decrease. A weak second-harmonic component is seen [14] after about 3.0

ns, growing to a peak value of 19% of the fundamental. For the small a_0 foil, contrast becomes observable after 2.0 ns, and grows exponentially until about 3.5 ns, after which the perturbation appears to grow linearly during this “drift” phase. A second harmonic is seen after ~ 3.5 ns, reaching 31% of the fundamental (though with a large uncertainty). An accelerated blank foil (no imposed surface perturbation) showed no contrast at any time. Defining an optical depth growth factor (GF_{OD}) as the ratio of maximum to initial contrast for the fundamental mode, we get $GF_{OD} = 6 \pm 1$, 22 ± 6 , and 75 ± 31 for the large, intermediate, and small a_0 foils, respectively. These growth factors are much larger than the $GF \leq 5$ observed with FS foils indirectly driven using 1-ns-square laser pulses [11]. The difference is attributed to the steep density gradient and extended acceleration [see Fig. 4(a)] with the shaped drive used in the present work.

The smooth curves shown in Fig. 4(b) represent two-dimensional LASNEX [15] simulations. The results of the simulations are postprocessed by transporting the measured backlighter x-ray spectrum through the calculated foil opacity, folding in the measured instrument responses. In addition to the x-ray backlighting resulting from the 5-ns laser pulse incident on a Rh disk, there is additional backlighting due to thermal emission from plasma filling the hohlraum. This latter component exists only as a short burst just after peak power of the drive lasers, and was measured on separate shots. Results of the calculated contrast, both with and without hohlraum emission in the backlighter spectrum, are shown in the figure. This short burst of added backlighting does not affect the interpretation of our results, and will be neglected in the remainder of our analysis. For large a_0 and to a lesser extent for intermediate a_0 , the calculated foils appear to burn through somewhat earlier in time than was observed. This most likely results from inadequate treatment of the detailed shape of the nonlinear spikes and bubbles, as agreement during the linear RT growth phase is excellent. Another possibility is the opacity modeling, since the amount of opacity in the hot blowoff plasma determines how much x-ray drive reaches the ablation front. We also note that in the simulations GF_{OD} is equivalent to the growth in areal density $\int \rho dz$ to better than 5%, since the ablated FS foil material maintains its opacity to the ~ 3 -keV backlighter x rays.

We next compare our measurements with classical growth [1], $a(t) = a_0 e^{\gamma_{cl} t}$, where $\gamma_{cl} = (ka)^{1/2}$, $k = 2\pi/\lambda_{perturb}$, and a is the foil acceleration. (The reduction of γ_{cl} due to the finite thickness of the foil [17] is a small effect, less than 7% for our experiments [14].) Integrating the growth rate over time using the time-dependent acceleration from the simulation shown in Fig. 4(a), we have calculated the number of classical e -foldings, $\int \gamma_{cl} dt$, for the small a_0 foil. The observed (and simulated) e foldings is about 60% of that predicted for classical growth, namely, $\gamma \approx 0.6\gamma_{cl}$. We have also compared our measurements with a simple expression incorporating ab-

lative flow across a density gradient [18],

$$\gamma = \alpha(ka)^{1/2} - \beta kv_a,$$

where $\alpha = (1 + kL)^{-1/2}$, L is the density gradient scale length ($L = \rho/\nabla\rho$), v_a is the ablation velocity ($v_a = \dot{m}/\rho A$, A being cross-sectional area), and β is a multiplier thought to be between 1 and 3. The Atwood number, to a good approximation, is set to 1 in this comparison. The data and simulation fall in between the e -folding curves for $\beta=1$ and $\beta=2$, reduction in growth rate due primarily to ablation. The effect of the density gradient is small, since $L \approx 1 \mu\text{m}$ during peak growth.

In conclusion, by amplitude scaling on radiatively accelerated foils, we have measured RT growth over an extended range, spanning the linear into the nonlinear RT regime. For large a_0 ($4.5 \mu\text{m}$), the RT instability is nonlinear from the onset, bubble-and-spike formation commences quickly, and only limited growth occurs: $\text{GF} = 6 \pm 1$. For small a_0 ($0.16 \mu\text{m}$), the instability does not enter the nonlinear phase until much later, and substantial exponential growth occurs: $\text{GF} = 75 \pm 31$. The intermediate a_0 ($0.8 \mu\text{m}$) case falls in between these two extremes, and $\text{GF} = 22 \pm 6$. Computer simulations indicate that growth factors in contrast are approximately the same as those for foil areal density. Comparing with the calculated classical e foldings, we conclude that the observed growth is about 60% of classical. Comparisons with an expression including the density gradient and ablation velocity suggest that ablation is the dominant mechanism by which growth is reduced. Foils accelerated by a shaped x-ray drive show substantially more perturbation growth than with a square drive, due to a steep density gradient at the ablation front and a sustained foil acceleration.

We wish to thank the dedicated staff and support personnel at Nova; E. M. Campbell, R. P. Drake, and J. Grun for critical readings of this manuscript prior to publication; S. Davidson, T. Perry, H. Kornblum, R. Kauffman, and D. W. Phillion for spectral and timing measurements; and S. Weber for simulations of the foil trajectory experiment. This work was performed under the auspices of the U.S. DOE by the Lawrence Livermore

National Laboratory under Contract No. W-7405-ENG-48.

-
- [1] S. Chandrasekhar, *Hydrodynamic and Hydromagnetic Stability* (Oxford Univ. Press, London, 1968), Chap. 10.
 - [2] J. Nuckolls *et al.*, *Nature* (London) **239**, 139 (1972).
 - [3] J. D. Lindl and W. C. Mead, *Phys. Rev. Lett.* **34**, 1273 (1975).
 - [4] S. E. Bodner, *Phys. Rev. Lett.* **33**, 761 (1974); D. B. Henderson, R. L. McCrory, and R. L. Morse, *Phys. Rev. Lett.* **33**, 205 (1974).
 - [5] E. M. Campbell, *Laser Part. Beams* **9**, 209 (1991).
 - [6] R. Sigel *et al.*, *Phys. Rev. Lett.* **65**, 587 (1990); R. Sigel *et al.*, *Phys. Rev. A* **38**, 5779 (1988).
 - [7] K. Niu *et al.*, *Laser Part. Beams* **9**, 293 (1991); N. A. Tahir and R. C. Arnold, *Phys. Fluids B* **3**, 1717 (1991).
 - [8] C. P. Verdon *et al.*, *Phys. Fluids* **25**, 1653 (1982); M. J. De, C. Henshaw, G. J. Pert, and D. L. Youngs, *Plasma Phys. Controlled Fusion* **29**, 405 (1987); S. E. Bodner, M. H. Emery, and J. H. Gardner, *Plasma Phys. Controlled Fusion* **29**, 1333 (1987).
 - [9] A. J. Cole *et al.*, *Nature* (London) **299**, 329 (1982); R. R. Whitlock *et al.*, *Phys. Rev. Lett.* **52**, 819 (1984).
 - [10] J. Grun *et al.*, *Phys. Rev. Lett.* **58**, 2672 (1987); M. Desselberger *et al.*, *Phys. Rev. Lett.* **65**, 2997 (1990).
 - [11] J. D. Kilkenny, *Phys. Fluids B* **2**, 1400 (1990).
 - [12] J. S. Wark *et al.*, *Appl. Phys. Lett.* **48**, 969 (1986); H. Nishimura *et al.*, *Phys. Fluids* **31**, 2875 (1988).
 - [13] R. J. Ellis *et al.*, *Rev. Sci. Instrum.* **61**, 2759 (1990).
 - [14] B. A. Remington *et al.*, LLNL Laser Program Winter Quarterly Report No. UCRL-LR-105821-91-1, 1990 (to be published), Vol. 1, No. 1, p. 7.
 - [15] G. B. Zimmerman and W. L. Kruer, *Comments Plasma Phys. Controlled Fusion* **2**, 51 (1975).
 - [16] David H. Munro, *Phys. Fluids B* **1**, 134 (1989); M. Tabak, D. H. Munro, and J. D. Lindl, *Phys. Fluids B* **2**, 1007 (1990); K. O. Mikaelian, *Phys. Rev. A* **42**, 4944 (1990); C. E. Max, C. F. McKee, and W. C. Mead, *Phys. Fluids* **23**, 1620 (1980).
 - [17] L. D. Landau and E. M. Lifshitz, *Fluid Mechanics* (Pergamon, New York, 1959), Sect. 12, Problem 3, p. 41.
 - [18] H. Takabe *et al.*, *Phys. Fluids* **28**, 3676 (1985); David H. Munro, *Phys. Rev. A* **38**, 1433 (1988).